NANO LETTERS

pubs.acs.org/NanoLett

Letter

Additive Manufacturing of High-Refractive-Index, Nanoarchitected Titanium Dioxide for 3D Dielectric Photonic Crystals

Andrey Vyatskikh, Ryan C. Ng, Bryce Edwards, Ryan M. Briggs, and Julia R. Greer*

Cite This: *Nano Lett.* 2020, 20, 3513−3520

Read Online

ACCESS | Metrics & More | Article Recommendations | Supporting Information

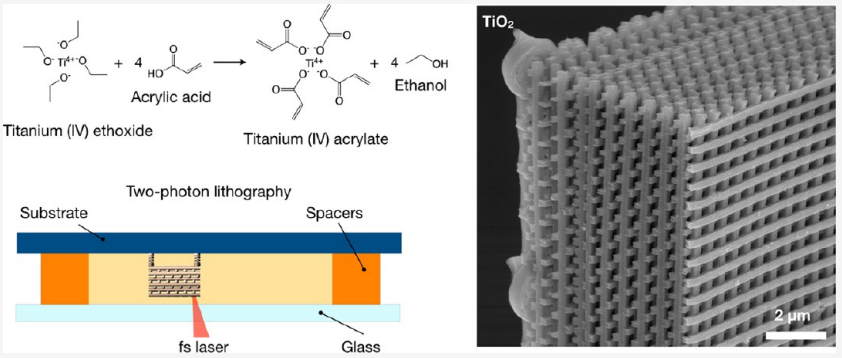

ABSTRACT: Additive manufacturing at small scales enables advances in micro- and nanoelectromechanical systems, micro-optics, and medical devices. Materials that lend themselves to AM at the nanoscale, especially for optical applications, are limited. State-of-the-art AM processes for high-refractive-index materials typically suffer from high porosity and poor repeatability and require complex experimental procedures. We developed an AM process to fabricate complex 3D architectures out of fully dense titanium dioxide (TiO_2) with a refractive index of 2.3 and nanosized critical dimensions. Transmission electron microscopy (TEM) analysis proves this material to be rutile phase of nanocrystalline TiO_2, with an average grain size of 110 nm and <1% porosity. Proof-of-concept woodpile architectures with 300−600 nm beam dimensions exhibit a full photonic band gap centered at 1.8−2.9 μm, as revealed by Fourier-transform infrared spectroscopy (FTIR) and supported by plane wave expansion simulations. The developed AM process enables advances in 3D MEMS, micro-optics, and prototyping of 3D dielectric PhCs.

KEYWORDS: *additive manufacturing, titanium dioxide, hybrid organic−inorganic material, two-photon lithography, high refractive index, photonic crystals*

Downloaded via UNIV OF EXETER on July 14, 2020 at 04:49:59 (UTC).
See https://pubs.acs.org/sharingguidelines for options on how to legitimately share published articles.

INTRODUCTION

Additive manufacturing (AM) represents a set of processes for layer-by-layer fabrication of 3D parts out of polymers, metals, and ceramics.[1−3] At the micro- and nanoscales, AM is poised to become the enabling technology for efficient 3D MEMS, microbattery electrodes, electrically small antennae, and micro-optical components.[4−7] Facilitating these technologies requires a fabrication process to create a variety of functional materials in 3D; however, the material choice for AM at the nano- and microscale is limited. This limitation is especially pronounced when particular material properties, including piezoelectric, magnetic, or optical, are required for the final application.[8−10]

A conspicuous example is a lack of AM processes for high-refractive-index (n), low-absorption materials with nanosized dimensions,[11] which are typically required for micro-optics and device applications. Polymer materials that can be shaped using direct laser writing (DLW) methods, such as two-photon lithography (TPL), are limited to refractive indices below 1.8.[12] Hybrid materials for TPL that consist of inorganic silica-type networks with embedded heteroatoms, including Zr, Zn, and Ge, have been demonstrated, but their refractive indices were below 1.6.[13−16] Direct laser writing (DLW) of As_2S_3 chalcogenide glasses with n between 2.45 and 2.53 in the infrared has been demonstrated by taking advantage of their photoinduced metastability,[9] but the high index mismatch between the lens and the printed material complicated the feature size control. Metal oxides with refractive indices $n \sim 1.9$ have been nanoarchitected using DLW of aqueous metal-containing photopolymers followed by calcination, but the low metal ion loading in these resins led to linear shrinkage of up to 87%, which made it challenging to preserve the complex 3D geometry.[8,17] TPL of organic−inorganic resists combined with

Received: February 2, 2020
Revised: April 22, 2020
Published: April 27, 2020

ACS Publications

© 2020 American Chemical Society

https://dx.doi.org/10.1021/acs.nanolett.0c00454
Nano Lett. 2020, 20, 3513−3520

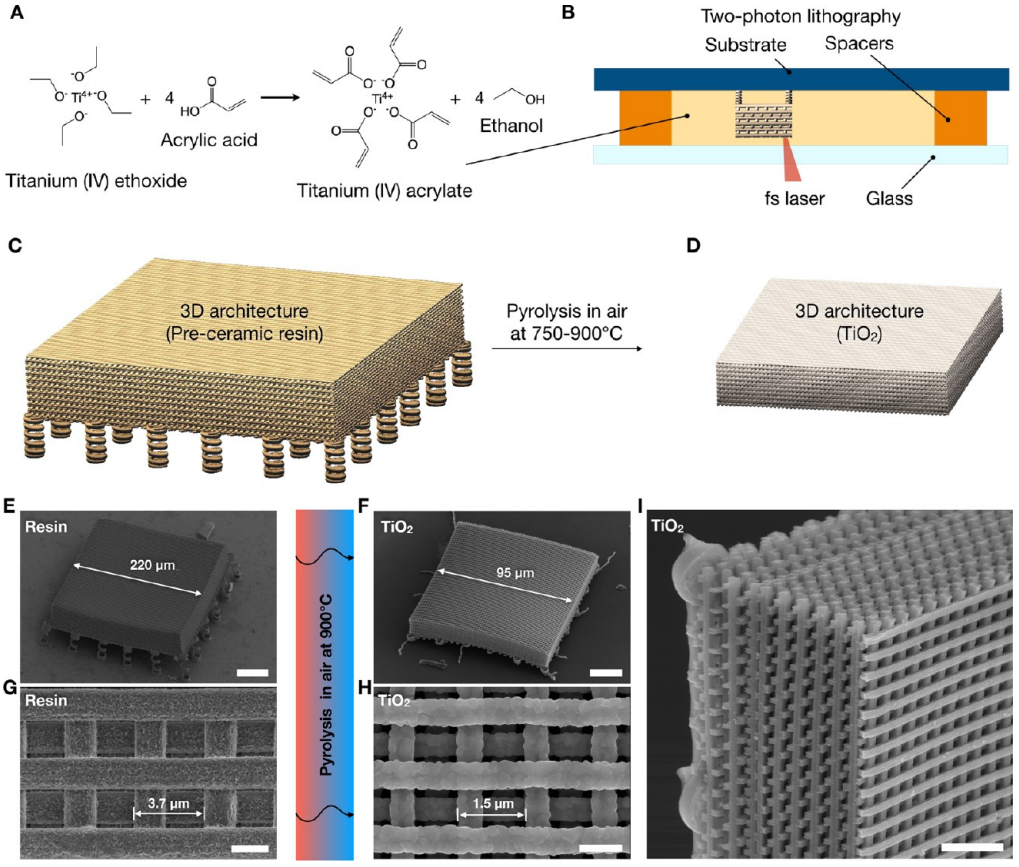

Figure 1. Process for nanoscale additive manufacturing (AM) of titanium dioxide and SEM characterization of as-fabricated TiO_2 3D architectures. (A) Ligand exchange reaction between titanium(IV) ethoxide and acrylic acid is used to synthesize a liquid TiO_2 precursor in the photopolymer. (B) Titania preceramic photopolymer is used in a two-photon lithography process to fabricate preceramic 3D architectures. (C) Schematic of a preceramic woodpile architecture supported by a set of springs that decouple it from the substrate. (D) Titania woodpile structure is formed by calcination of the preceramic part. (E, G) Representative SEM images of preceramic woodpile architectures. (F, H, I) Representative TiO_2 woodpile architectures after calcination at 750−900 °C. Scale bars are 50 μm for panel E, 20 μm for F, 2 μm for G, 1 μm for H, and 2 μm for I.

a postlithography thermal treatment has shown promise to create 3D nanolattices of metals and ceramics, but the residual porosity of up to 20% within the beams reduced the effective refractive index.[18,19] An AM process that can repeatably and accurately produce 3D architectures with submicron geometrical features out of high-refractive-index, low-absorption material is yet to be developed and would realize multiple micro-optical devices and three-dimensional (3D) dielectric photonic crystals (PhCs).[10]

3D dielectric PhCs have been a focus of extensive research for their unique ability to tailor and manipulate light.[20,21] 3D PhCs with a full photonic band gap,[22,23] 3D chiral PhCs that control light polarization,[24] and all-angle negative refractive (AANR) index materials[25] have been demonstrated. All of these devices are enabled by satisfying stringent optical material requirements and dimensional control. For example, obtaining a full photonic band gap in woodpile architectures requires constituent materials with a refractive index $n \gtrsim 1.9$,[26] and attaining AANR requires an effective index of $n \geq 2.49$,[27] with individual features smaller than the target wavelength. Creating nanosized three-dimensional architectures out of high-refractive-index materials, such as silicon (Si), gallium arsenide (GaAs), and titanium dioxide (TiO_2), can only be achieved via sophisticated experimental procedures. Examples include micromanipulation of individually stacked layers[28] or single- or double-inversion of a polymer template that often result in features with up to 16% porosity.[10,23]

Titanium dioxide (titania, TiO_2) represents a beneficial material choice for 3D dielectric PhCs in the visible and the infrared because of its high refractive index and high transparency.[10] The highest refractive index, between 2.45 and 3.03 for 500−1500 nm wavelengths, is attained in the rutile phase of TiO_2.[29] The processes for AM of titania demonstrated to date suffer from high porosity, low refractive index of the constituent material, and poor repeatability. An ideal AM process for titania would have to repeatably and accurately produce 3D structures with submicron features out of fully dense rutile TiO_2. Several previous studies have described AM processes for TiO_2. Direct ink writing (DIW) of sol−gel inks followed by calcination has been shown to produce TiO_2 features with submicron dimensions that are ∼10% porous and contained about a half of a lower-index anatase phase, which lowered their effective refractive index by at least 10%.[30] Femtosecond laser processing of liquid TiO_2 precursors has been used to selectively introduce insoluble regions into the patterned material by breaking chemical bonds, but the poor adhesion between the sample and the substrate led to the loss of heat-treated 3D structures.[18] Laser-induced decomposition of sol−gel precursors enabled 2D patterning of TiO_2/carbon composites with typical feature widths of 3 μm for crystalline TiO_2 and has not been extended

https://dx.doi.org/10.1021/acs.nanolett.0c00454
Nano Lett. 2020, 20, 3513−3520

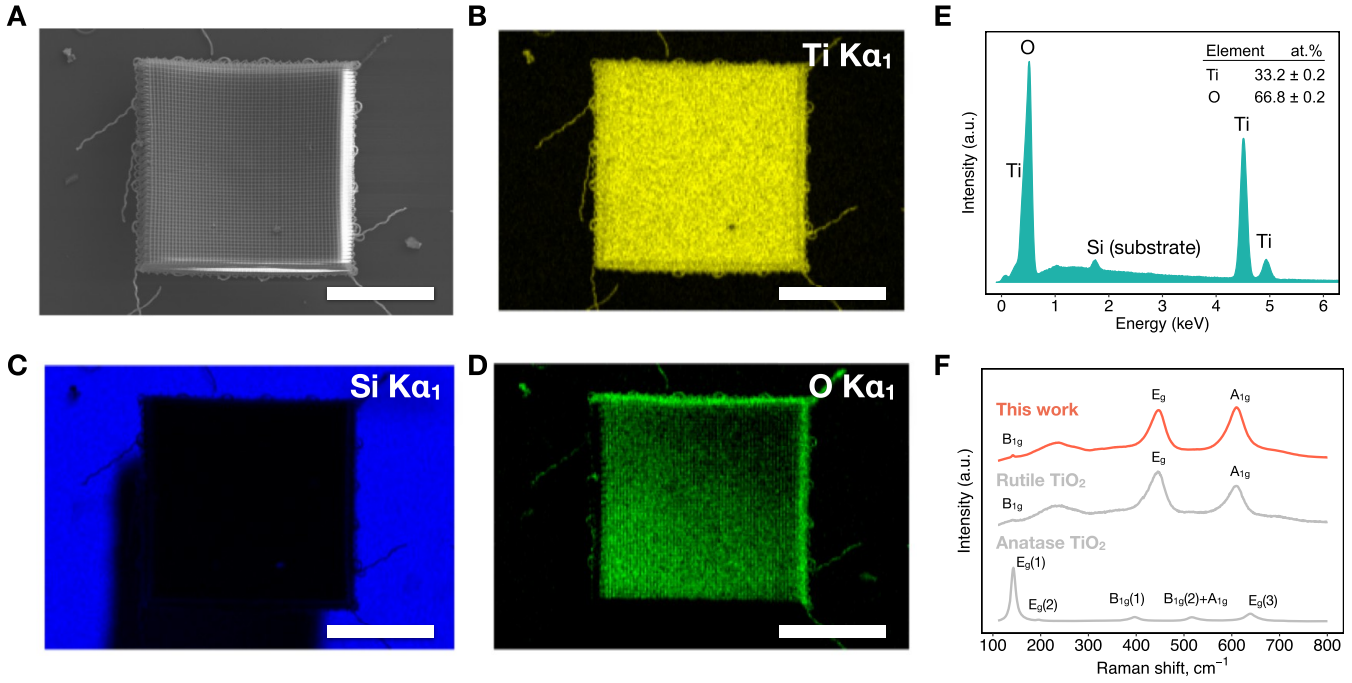

Figure 2. Characterization of chemical composition and phase of TiO_2 using SEM EDS and Raman spectroscopy. (A–D) SEM EDS mapping of a representative woodpile architecture fabricated on a silicon substrate reveals a uniform distribution of titanium and oxygen. (E) The estimation of chemical composition from a representative EDS spectrum shows a 1:2 atom % ratio of titanium to oxygen consistent with TiO_2. (F) Raman spectrum of as-fabricated TiO_2 compared to reference spectra of rutile and anatase. Scale bars are 50 μm for panels A–D.

to three dimensions.[31] Using hybrid organic–inorganic materials in AM has been demonstrated for a stereolithography (SLA)-based patterning to create architected titania with 150 μm feature sizes. However, this process could not be extended to submicron features due to the resolution limit of SLA.[32] We previously showed feasibility of AM of 3D nanoarchitected titania using two-photon lithography; this approach did not achieve precise dimensional control required for the emergence of a full photonic band gap.[33]

Here, we demonstrate an AM process capable of repeatably and accurately producing 3D nanoarchitected titanium dioxide with critical feature dimensions between 150 and 600 nm and <1% porosity. We synthesize a hybrid organic–inorganic precursor to formulate a preceramic TiO_2 resist. We then use two-photon lithography to pattern the designed 3D structures and pyrolyze them at 750–900 °C in air. This process shrinks the dimensions of originally patterned 3D nanoarchitectures by ~60% to produce fully dense nanocrystalline TiO_2 replicas. As a proof of concept, we created 3D dielectric PhCs using this process by fabricating rutile TiO_2 patterned into woodpile face-centered tetragonal (FCT) architectures with beam dimensions of 300–600 nm and lateral periods of 0.8–1.5 μm. We use plane wave expansion (PWE) simulations and Fourier-transform infrared spectroscopy (FTIR) to demonstrate the full photonic band gaps centered at 1.8–2.9 μm. This AM process for fabricating 3D nanoarchitected fully dense TiO_2 will be crucial for rapid prototyping and manufacturing of 3D PhCs and micro-optical devices.

RESULTS

Process for AM of 3D Nanoarchitected Titania. To prepare titania preceramic photopolymer, we first used a ligand exchange reaction between titanium(IV) ethoxide and acrylic acid in a 1:4 molar ratio to synthesize titanium(IV) acrylate (Figure 1A). The reaction was conducted in a glovebox to minimize exposure to oxygen and water. The resulting hybrid organic–inorganic TiO_2 precursor can be embedded in a polymer network during free-radical polymerization. When combined with an acrylic monomer, pentaerythritol triacrylate, the solution becomes clear and orange. A two-photon photoinitiator, 7-diethylamino-3-thenoylcoumarin (DETC), was then dissolved in dichloromethane and added to the solution (see Methods in the SI); the resulting liquid photoresist was drop cast onto a silicon substrate and 3D printed in a TPL system (Photonic Professional GT, Nanoscribe GmbH). Architected samples were designed to rest on top of a 2D lattice layer supported by a spring-and-pillars array that decoupled the architecture from the substrate during pyrolysis and minimized its distortion during shrinkage[19,33] (Figure 1B,C). Nonpolymerized resist was washed away, and freestanding architectures were pyrolyzed in air at 900 °C for 1 h (see Methods in the SI) to create replicas of the original structures, with a concomitant ~60% reduction in dimensions, made entirely out of titanium dioxide (Figure 1D).

Feature Dimensions. To ensure high accuracy of geometric dimensions in devices fabricated using this AM process, we systematically studied the influence of process parameters on the size of the individual features. Previous studies[34–36] reported strong nonlinear dependence of the dimensions of the polymerized material, or voxel, on the laser power (LP) and the exposure time (ET) in two-photon lithography, which is unique for each photopolymer. We used ascending scan experiments[34] to evaluate the voxel width and height for this hybrid photoresist for LP between 12.5 and 20 mW and ET between 0.5 and 10 ms. Figure S1 shows that, for ET between 1 and 10 ms at 20 mW, the voxel width varied

https://dx.doi.org/10.1021/acs.nanolett.0c00454
Nano Lett. 2020, 20, 3513–3520

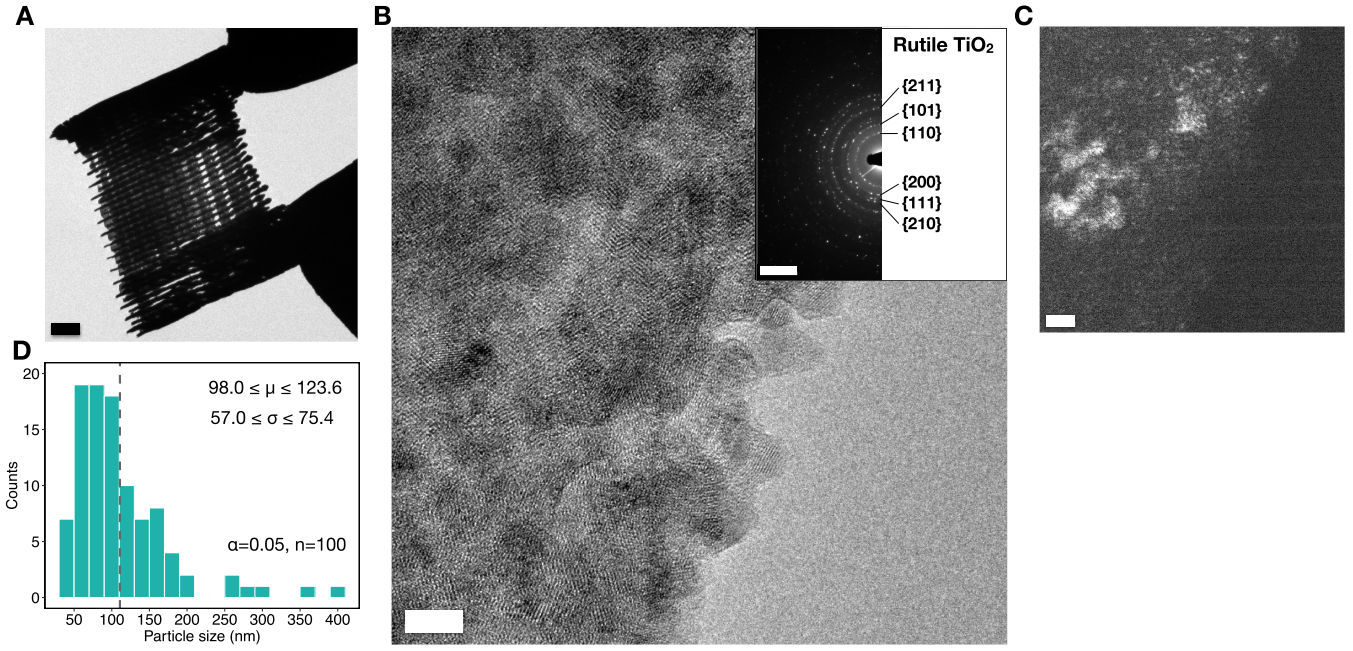

Figure 3. TEM characterization of as-fabricated TiO_2 3D architectures. (A) Low-magnification TEM image showing a 100 nm thick cross-section of a TiO_2 woodpile structure prepared using an FIB lift-out procedure. (B) An HRTEM image of a cross-section of an individual beam, an electron diffraction pattern (inset), and (C) a corresponding dark-field TEM image reveal that the beams consist predominantly out of nanocrystalline rutile TiO_2. (D) Grain size histogram for n = 100 particles measured from an SEM image showing 95% confidence intervals on the mean grain size (μ) and the standard deviation (σ). Scale bars are 2 μm for panel A, 5 nm for B and C, and 2 nm^{-1} for B, inset.

from 440 to 560 nm; its height changed from 1.6 to 3.2 μm, and the voxel aspect ratio varied from 3.8 to 5.3.

To predict and reliably control the feature size for 3D photonic crystal fabrication, we adopted a model by Serbin et al.[35] that links the voxel dimensions in a two-photon lithography process to the laser exposure parameters (see the Supporting Information). Voxel height L (eq 1) and voxel width d (eq 2) can be expressed as

$$L = 2z_R\sqrt{\sqrt{\alpha t P^2} - 1} \quad (1)$$

$$d = w_0\sqrt{\log[\alpha t P^2]} \quad (2)$$

where z_R is the Rayleigh distance of the objective [m], w_0 is the laser beam waist [m], and $\alpha t P^2$ is a nondimensional parameter where t is the exposure time [s], P is the laser power [W], and α is a constant that depends on the exposure pattern and the photopolymer formulation (see the Supporting Information). Figure S1 demonstrates that experimentally measured voxel dimensions are in good agreement with this model, which provides a quantifiable way to tailor the laser exposure parameters to achieve target feature dimensions.

Accuracy and Repeatability of Geometric Features. We demonstrate the efficiency of this approach by fabricating 3D architectures with tetragonal woodpile geometry that has overall dimensions of 220 × 220 μm, a lateral period x_L of 3.7 μm, an axial factor (defined as the ratio of the axial period x_a to the lateral period x_L) of 1.1, and rectangular beams with 1.3 × 1.5 μm cross-sections. Figure 1F,G shows SEM images of a representative woodpile structure after pyrolysis that contains 60 periods in the lateral direction and 9 periods in the axial direction. The beams in this sample had 530 × 600 nm rectangular cross-sections and a lateral period of 1.47 μm, and overall lateral dimensions were 95 × 95 μm. The features appeared to be uniform, and the shrinkage postpyrolysis appeared to be isotropic.

To quantify the effect of shrinkage on geometrical distortions within the structure, we analyzed the variability of geometric dimensions in axial (Figure S2) and lateral directions in the woodpile using SEM measurements (Table S1). We found that in the axial direction the lateral period did not vary by more than 5%, with no statistically significant deviations in the average beam width (Figure S2). In the lateral direction, we analyzed the variability of the lateral period using nested variance analysis,[37] which revealed a total variability of 25 nm, or 1.7% of the target dimension, across the entire sample (Table S2). We also found that the contribution of spatial variability of the lateral period was only 13 nm, or less than 1% of the target (Table S2).

Material Characterization. To characterize the chemical composition of as-fabricated material, we conducted energy-dispersive X-ray spectroscopy (EDS) on a representative sample with in-plane dimensions of 95 × 95 μm and a lateral period of 1.5 μm (Figure 2A). SEM EDS maps (Figure 2B–D) show a uniform distribution of Ti and O throughout the structure with no apparent segregations into titanium- or oxygen-rich phases. EDS spectra taken from a 20 × 20 μm area in the center of the sample (Figure 2E) reveal the chemical composition to be 66.8 at. % oxygen and 33.2 at. % titanium. Silicon substrate was excluded from the composition estimate.

To evaluate the phase composition, Raman spectra were collected from the as-fabricated 3D architectures using a 514 nm laser focused through a 50× microscope objective. Figure 2F shows a representative Raman spectrum along with the reference spectra collected from rutile and anatase samples (see Methods in the SI). The Raman signature revealed peaks at 145, 448, and 613 cm^{-1} that match the rutile TiO_2 reference spectrum.

https://dx.doi.org/10.1021/acs.nanolett.0c00454
Nano Lett. 2020, 20, 3513−3520

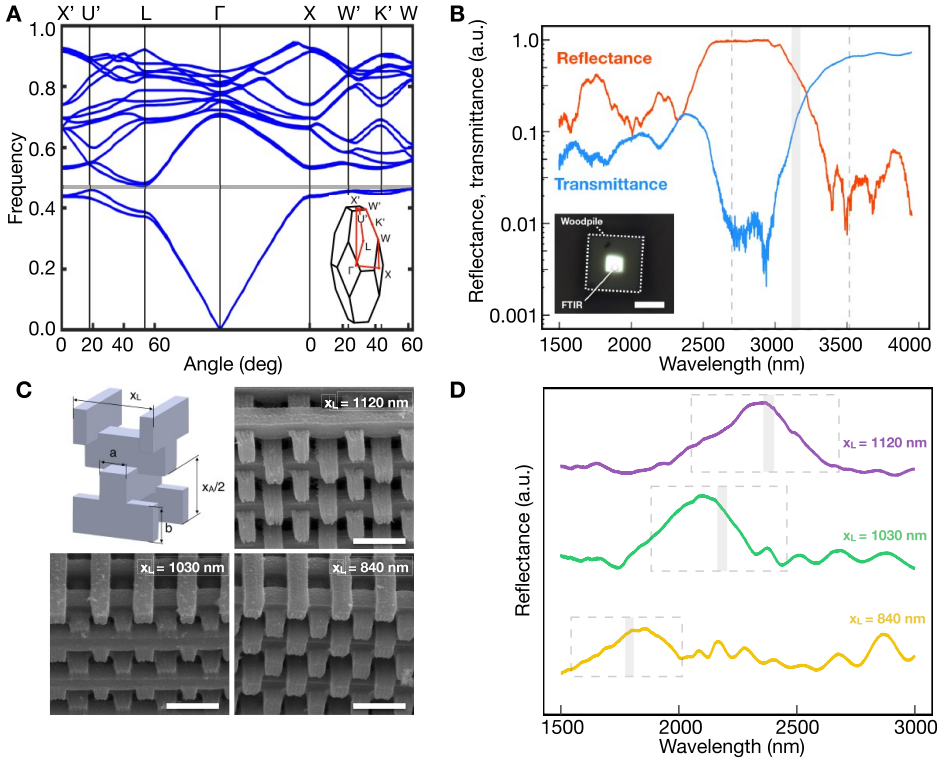

Figure 4. Optical characterization of 3D photonic crystals fabricated using the developed nanoscale AM process. (A) Calculated band structure of the fabricated woodpile FCT architecture. The gray band shows the position of a full photonic band gap. (B) FTIR reflectance and transmittance spectra taken from a woodpile structure showing the emergence of high reflectance and low transmittance bands centered at ~2.9 μm. (C) A schematic of a woodpile unit cell and SEM of representative woodpile structures with 1120, 1030, and 840 nm lateral periods fabricated using the developed AM method. (D) FTIR reflectance spectra for as-fabricated woodpile structures with varying periodicities showing passive tuning of the reflectance band position between 1.8 and 2.4 μm. Scale bars are 1 μm for panel C.

We analyzed the atomic-level microstructure of as-fabricated TiO_2 structures using transmission electron microscopy (TEM) and electron diffraction. We prepared a 100 nm thick cross-section of a sample whose beams had 960 × 150 nm elliptical cross-sections, lateral periodicities of 1090 nm, and a footprint of 70 × 70 μm using a focused ion beam (FIB) lift-out procedure (Figure 3A). High-resolution (Figure 3B) and dark-field (Figure 3C) TEM images reveal that a typical beam cross-section is >99% dense and is composed of nanocrystallites with a mean size of 110 nm (see Figure 3D, and Figures S3 and S4). The electron diffraction pattern (Figure 3B, inset) confirms the crystalline phase of TiO_2 to be rutile.

Optical Behavior. We used plane wave expansion (PWE) simulations and Fourier-transform infrared spectroscopy (FTIR) measurements to investigate the optical behavior of TiO_2 woodpiles. We chose experimentally equivalent geometric parameters extracted from images in Figure 1F,H and a refractive index of 2.3, obtained by ellipsometry measurements on as-fabricated films (Figure S5) for PWE simulations. Figure 4A shows the band diagram with the corresponding Brillouin zone (inset) calculated for an FCT woodpile architecture with these properties, which exhibits a full photonic band gap between frequencies of $0.465(2\pi c/x_L)$ and $0.474(2\pi c/x_L)$ (see Figure S6), where x_L is the lateral period of the woodpile, and c is the speed of light. Woodpiles with x_L of 1.47 μm have gap edges at 3.10 and 3.16 μm (Table S2).

To probe the simulation results experimentally, we measured the reflectance and transmittance of the as-fabricated woodpiles using FTIR with a Cassegrain objective with an angle range between 16° and 35.5° within a 30 × 30 μm area at the center of the sample. Previous experimental studies revealed that the position of FTIR reflectance bands is influenced by the stop-band positions that are being probed simultaneously at off-normal light incidences.[23] We calculated the expected stop-band edges from the woodpile band diagram probed along X′−U′−L and X′−W′−K′ at experimental off-normal incidence angles to be between $0.418(2\pi c/x_L)$ and $0.544(2\pi c/x_L)$, which corresponds to the wavelengths of 2.7−3.5 μm (Table S2). Figure 4B contains FTIR spectra that reveal a high reflectance/low transmittance band centered at ~2.9 μm, plotted along with the computed position of a full photonic band gap (gray rectangle) and the range of stop-band positions for the 16−35.5° incidence angles (vertical dash lines). The position of the high reflectance band was found to be within 7% from the expected full photonic band gap.

Varying the TiO_2 precursor loading in the photopolymer enables control over the amount of postpyrolysis linear shrinkage and of the structural feature sizes, which enables access to multiple wavelengths. We fabricated 3D photonic crystals with reduced lateral periods of 1.12, 1.03, and 0.84 μm by starting with the same preceramic 3D sample and varying the TiO_2 precursor loading by 50−83% (Figure 4C). These structures were replicas of the titania woodpiles with x_L = 1.47 μm shown in Figure 1F. Figure 4D shows FTIR reflectance spectra for these samples, as well as the computed band gap positions, that revealed high reflectance bands centered at 1.8, 2.2, and 2.4 μm, which are within 0.3%, 4.8%, and 3.0% of the target full photonic band gap positions (Table S2).

https://dx.doi.org/10.1021/acs.nanolett.0c00454
Nano Lett. 2020, 20, 3513−3520

DISCUSSION

We developed an AM process to produce three-dimensional networks of fully dense submicron features out of a transparent, high-refractive-index material that can be used to fabricate 3D dielectric photonic crystals. Compositional and microstructural analysis suggests that the as-fabricated material is composed of fully dense nanocrystalline rutile TiO_2 with minimal carbon content. EDS revealed the chemical composition of 33.2 at. % Ti and 66.8 at. % O, which corresponds to a 1:2 atomic ratio of Ti to O characteristic of titanium dioxide. It was not possible to accurately determine the C content using EDS because of its low sensitivity to light elements and because of inevitable carbon contamination in the SEM chamber.[38] Inclusion of the carbon peak in the EDS spectrum fit did not result in the fit improvement, which further corroborates extremely low atom % C. Processes based on laser-driven formation of TiO_2/carbon composites yielded a substantial amount of carbon[31] that can lower the material transparency.

Electron diffraction and Raman spectroscopy identified TiO_2 to be in its rutile phase. The Raman spectrum taken from a representative architected sample revealed peaks that are in good agreement with first-order vibration modes found in rutile titania[39] (B_{1g} at 145 cm^{-1}, E_g at 448 cm^{-1}, and A_{1g} at 613 cm^{-1}), as well as with characteristic second-order scattering around 240 cm^{-1} (see Figure 2F). This finding is also consistent with other works that studied phase transformation in sol–gel derived titanium dioxide.[30,40] For example, dry sol–gels of TiO_2 were found to convert from anatase into rutile at 550 °C, with full transformation occurring at 800 °C.[40] These studies suggest rutile as the predominant expected phase of titania resulting from a heat treatment at 900 °C. Previous attempts to develop a titania AM process resulted in partially converted TiO_2 (e.g., rutile/anatase mix of 47 wt %/53 wt % in ref 30) and porous features with 10–16% air content,[10,30] which lowered the effective refractive index of individual features.

The ability to predict and reliably control the feature size based on the exposure parameters was critical for fabrication of 3D photonic crystals. Estimating polymerization volume in two-photon lithography generally requires numerical simulations that take into account radical generation and inhibition, oxygen diffusion, local heating, and many other factors.[36] We studied the dependence of the voxel dimensions on the exposure parameters by examining polymerization kinetics inside the voxel volume at millisecond time scales. Mueller et al.[41] experimentally showed that at exposure times between 1 and 10 ms two-photon polymerization is primarily driven by radical generation. Uppal et al. found that the generated radicals remain mostly confined to the voxel volume during the exposure.[36] Mueller et al.[42] have demonstrated that the temperature inside the polymerizing voxel did not increase by more than 5 K at 20 mW laser power. These previous studies allowed us to adopt a closed-form solution derived by Serbin et al. for an isothermal system with no diffusion to predict the voxel dimensions in our system.

FTIR reflectance and transmittance spectra of four woodpile samples (Figure 4B,D) revealed that the observed high reflectance peaks were centered within 0.3–7% from the expected position of full photonic band gaps predicted by PWE (Figure 4A). The observed deviations can be attributed to (i) the variability of geometric dimensions throughout the sample and (ii) the uncertainty of the refractive index measured by ellipsometry and used in PWE simulations. The SEM measurements and nested variance analysis showed ~1% in-plane (Table S1) and ~5% out-of-plane (Figure S2) deviations of the lateral period throughout the woodpile, and the measured refractive index of a TiO_2 film of 2.3 is 4–15% lower than the expected index of 2.40–2.71 for rutile TiO_2 within a 1500–3000 nm range.[29] This could be caused by some inherent porosity in the TiO_2 film (Figure S5, left) used for the ellipsometry measurements; the beams that comprise TiO_2 PhCs are fully dense. Uncertainty in the geometrical dimensions of up to 5% and in the refractive index of up to 15% can contribute to the observed deviations between experimental and simulated peak positions.

In summary, we developed an additive manufacturing process to create 3D nanoarchitected titania with a submicron resolution. We demonstrate the feasibility and efficiency of this process using a woodpile FCT architecture with individual feature widths of 150 nm as a model system. The as-fabricated material is nearly carbon-free and consists of homogeneous, fully dense nanocrystalline rutile TiO_2. Taking advantage of the high refractive index and transparency of titania, we prototyped several PhCs with submicron lateral periods and full photonic band gaps centered at 1.8–2.9 μm, consistently confirmed by PWE simulations and FTIR measurements. Fabricating PhCs with full photonic band gaps in the visible requires lateral periods of ~300 nm,[10] which can be achieved by modulating precursor loading. We showed that using lower concentrations of TiO_2 precursor allows for 2 times smaller features due to higher postpyrolysis linear shrinkage. The developed freeform AM process is not limited to woodpile geometries and can be applied to directly fabricate a broad range of 3D architectures. This nanoscale AM process is not limited to TiO_2: other hybrid organic–inorganic-based photopolymers can be formulated to print a variety of materials, including other dielectrics, metals, and semiconductors. AM of 3D nanoarchitected titania is poised to enable facile fabrication of components for a much broader set of applications, including micro-optics, 3D MEMS, and minimally invasive tools and procedures.

ASSOCIATED CONTENT

Supporting Information

The Supporting Information is available free of charge at https://pubs.acs.org/doi/10.1021/acs.nanolett.0c00454.

Materials and methods, voxel shape modeling, and additional data and figures including voxel dimensions, beam widths and lateral positions, SEM images, a crystal size distribution, TEM images, and a band diagram (PDF)

AUTHOR INFORMATION

Corresponding Author

Julia R. Greer – *Division of Engineering and Applied Science, California Institute of Technology, Pasadena, California 91125, United States*; Email: jrgreer@caltech.edu

Authors

Andrey Vyatskikh – *Division of Engineering and Applied Science, California Institute of Technology, Pasadena, California 91125, United States*; orcid.org/0000-0002-6917-6931

https://dx.doi.org/10.1021/acs.nanolett.0c00454
Nano Lett. 2020, 20, 3513–3520

Ryan C. Ng − *Division of Chemistry and Chemical Engineering, California Institute of Technology, Pasadena, California 91125, United States;* orcid.org/0000-0002-0527-9130

Bryce Edwards − *Division of Engineering and Applied Science, California Institute of Technology, Pasadena, California 91125, United States*

Ryan M. Briggs − *Jet Propulsion Laboratory, California Institute of Technology, Pasadena, California 91109, United States*

Complete contact information is available at: https://pubs.acs.org/10.1021/acs.nanolett.0c00454

Notes

The authors declare no competing financial interest.

■ ACKNOWLEDGMENTS

The authors are grateful for the support of J.R.G.'s DoD Vannevar-Bush Faculty Fellowship. Authors also acknowledge A.V.'s Resnick Sustainability Institute at Caltech Fellowship and NIH Biotechnology Leadership Pre-Doctoral Training Program support. We thank Professor George R. Rossman (Caltech) for his assistance with Raman spectroscopy and FTIR.

■ REFERENCES

(1) Zocca, A.; Colombo, P.; Gomes, C. M.; Günster, J. Additive Manufacturing of Ceramics: Issues, Potentialities, and Opportunities. *J. Am. Ceram. Soc.* **2015**, *98* (7), 1983−2001.

(2) Melchels, F. P. W.; Domingos, M. A. N.; Klein, T. J.; Malda, J.; Bartolo, P. J.; Hutmacher, D. W. Additive Manufacturing of Tissues and Organs. *Prog. Polym. Sci.* **2012**, *37* (8), 1079−1104.

(3) Frazier, W. E. Metal Additive Manufacturing: A Review. *J. Mater. Eng. Perform.* **2014**, *23* (6), 1917−1928.

(4) Hirt, L.; Reiser, A.; Spolenak, R.; Zambelli, T. Additive Manufacturing of Metal Structures at the Micrometer Scale. *Adv. Mater.* **2017**, *29*, 1604211.

(5) Vaezi, M.; Seitz, H.; Yang, S. A Review on 3D Micro-Additive Manufacturing Technologies. *Int. J. Adv. Manuf. Technol.* **2013**, *67* (5), 1721−1754.

(6) Pikul, J. H.; Gang Zhang, H.; Cho, J.; Braun, P. V.; King, W. P. High-Power Lithium Ion Microbatteries from Interdigitated Three-Dimensional Bicontinuous Nanoporous Electrodes. *Nat. Commun.* **2013**, *4*, 1732.

(7) Nelson, B. J.; Kaliakatsos, I. K.; Abbott, J. J. Microrobots for Minimally Invasive Medicine. *Annu. Rev. Biomed. Eng.* **2010**, *12* (1), 55−85.

(8) Yee, D. W.; Lifson, M. L.; Edwards, B. W.; Greer, J. R. Additive Manufacturing of 3D-Architected Multifunctional Metal Oxides. *Adv. Mater.* **2019**, *31*, 1901345.

(9) Wong, S.; Deubel, M.; Pérez-Willard, F.; John, S.; Ozin, G. A.; Wegener, M.; Von Freymann, G. Direct Laser Writing of Three-Dimensional Photonic Crystals with a Complete Photonic Bandgap in Chalcogenide Glasses. *Adv. Mater.* **2006**, *18* (3), 265−269.

(10) Frölich, A.; Fischer, J.; Zebrowski, T.; Busch, K.; Wegener, M. Titania Woodpiles with Complete Three-Dimensional Photonic Bandgaps in the Visible. *Adv. Mater.* **2013**, *25* (26), 3588−3592.

(11) Camposeo, A.; Persano, L.; Farsari, M.; Pisignano, D. Additive Manufacturing: Applications and Directions in Photonics and Optoelectronics. *Adv. Opt. Mater.* **2019**, *7* (1), 1800419.

(12) Liu, J.; Ueda, M. High Refractive Index Polymers: Fundamental Research and Practical Applications. *J. Mater. Chem.* **2009**, *19* (47), 8907.

(13) Haas, K. H.; Wolter, H. Synthesis, Properties and Applications of Inorganic-Organic Copolymers (ORMOCER®s). *Curr. Opin. Solid State Mater. Sci.* **1999**, *4* (6), 571−580.

(14) Jonušauskas, L.; Gailevičius, D.; Mikoliunaite, L.; Sakalauskas, D.; Šakirzanovas, S.; Juodkazis, S.; Malinauskas, M. Optically Clear and Resilient Free-Form μ-Optics 3D-Printed via Ultrafast Laser Lithography. *Materials* **2017**, *10* (1), 12.

(15) Yeh, C. C.; Liu, H. C.; Heni, W.; Berling, D.; Zan, H. W.; Soppera, O. Chemical and Structural Investigation of Zinc-Oxo Cluster Photoresists for DUV Lithography. *J. Mater. Chem. C* **2017**, *5*, 2611.

(16) Malinauskas, M.; Ukauskas, A.; Purlys, V.; Gaidukeviiut, A.; Baleviius, Z.; Piskarskas, A.; Fotakis, C.; Pissadakis, S.; Gray, D.; Gadonas, R.; et al. 3D Microoptical Elements Formed in a Photostructurable Germanium Silicate by Direct Laser Writing. *Opt. Lasers Eng.* **2012**, *50* (12), 1785−1788.

(17) Bond, W. L. Measurement of the Refractive Indices of Several Crystals. *J. Appl. Phys.* **1965**, *36* (5), 1674−1677.

(18) Passinger, S.; Saifullah, M. S. M.; Reinhardt, C.; Subramanian, K. R. V.; Chichkov, B. N.; Welland, M. E. Direct 3D Patterning of TiO2 Using Femtosecond Laser Pulses. *Adv. Mater.* **2007**, *19* (9), 1218−1221.

(19) Vyatskikh, A.; Delalande, S.; Kudo, A.; Zhang, X.; Portela, C. M.; Greer, J. R. Additive Manufacturing of 3D Nano-Architected Metals. *Nat. Commun.* **2018**, *9* (1), 593.

(20) John, S. Strong Localization of Photons in Certain Disordered Dielectric Superlattices. *Phys. Rev. Lett.* **1987**, *58* (23), 2486−2489.

(21) Yablonovitch, E. Inhibited Spontaneous Emission in Solid-State Physics and Electronics. *Phys. Rev. Lett.* **1987**, *58* (20), 2059−2062.

(22) Noda, S.; Tomoda, K.; Yamamoto, N.; Chutinan, A. Full Three-Dimensional Photonic Bandgap Crystals at Near-Infrared Wavelengths. *Science (Washington, DC, U. S.)* **2000**, *289* (5479), 604−606.

(23) Staude, I.; Thiel, M.; Essig, S.; Wolff, C.; Busch, K.; von Freymann, G.; Wegener, M. Fabrication and Characterization of Silicon Woodpile Photonic Crystals with a Complete Bandgap at Telecom Wavelengths. *Opt. Lett.* **2010**, *35* (7), 1094−1096.

(24) Von Freymann, G.; Ledermann, A.; Thiel, M.; Staude, I.; Essig, S.; Busch, K.; Wegener, M. Three-Dimensional Nanostructures for Photonics. *Adv. Funct. Mater.* **2010**, *20* (7), 1038−1052.

(25) Luo, C.; Johnson, S. G.; Joannopoulos, J. D. All-Angle Negative Refraction in a Three-Dimensionally Periodic Photonic Crystal. *Appl. Phys. Lett.* **2002**, *81* (13), 2352−2354.

(26) Ho, K. M.; Chan, C. T.; Soukoulis, C. M.; Biswas, R.; Sigalas, M. Photonic Band Gaps in Three Dimensions: New Layer-by-Layer Periodic Structures. *Solid State Commun.* **1994**, *89* (5), 413−416.

(27) Chernow, V. F.; Ng, R. C.; Greer, J. R. Designing Core-Shell 3D Photonic Crystal Lattices for Negative Refraction. *Proc. SPIE* **2017**, 101120G.

(28) Aoki, K.; Guimard, D.; Nishioka, M.; Nomura, M.; Iwamoto, S.; Arakawa, Y. Coupling of Quantum-Dot Light Emission with a Three-Dimensional Photonic-Crystal Nanocavity. *Nat. Photonics* **2008**, *2* (11), 688−692.

(29) Ribarsky, M. W. Titanium Dioxide (TiO2) (Rutile); In *Handbook of Optical Constants of Solids*; Palik, E. D., Ed.; Academic Press: Burlington, 1997; pp 795−804. DOI: 10.1016/B978-012544415-6.50042-X.

(30) Duoss, E. B.; Twardowski, M.; Lewis, J. A. Sol-Gel Inks for Direct-Write Assembly of Functional Oxides. *Adv. Mater.* **2007**, *19* (21), 3485−3489.

(31) Yu, S.-Y.; Schrodj, G.; Mougin, K.; Dentzer, J.; Malval, J.-P.; Zan, H.-W.; Soppera, O.; Spangenberg, A. Direct Laser Writing of Crystallized TiO2 and TiO2/Carbon Microstructures with Tunable Conductive Properties. *Adv. Mater.* **2018**, *30* (51), 1805093.

(32) Vyatskikh, A.; Kudo, A.; Delalande, S.; Greer, J. R. Additive Manufacturing of Polymer-Derived Titania for One-Step Solar Water Purification. *Mater. Today Commun.* **2018**, *15* (March), 288−293.

(33) Vyatskikh, A.; Ng, R. C.; Edwards, B.; Greer, J. R. Additive Manufacturing of Titanium Dioxide for Dielectric Photonic Crystals. *Proc. SPIE* **2019**, *10930*, 109300H.

(34) Sun, H. B.; Tanaka, T.; Kawata, S. Three-Dimensional Focal Spots Related to Two-Photon Excitation. *Appl. Phys. Lett.* **2002**, *80* (20), 3673−3675.

(35) Serbin, J.; Egbert, A.; Ostendorf, A.; Chichkov, B. N.; Houbertz, R.; Domann, G.; Schulz, J.; Cronauer, C.; Fröhlich, L.; Popall, M. Femtosecond Laser-Induced Two-Photon Polymerization of Inorganic−Organic Hybrid Materials for Applications in Photonics. *Opt. Lett.* **2003**, *28* (5), 301.
(36) Uppal, N. Modeling of Temperature-Dependent Diffusion and Polymerization Kinetics and Their Effects on Two-Photon Polymerization Dynamics. *J. Micro/Nanolithogr., MEMS, MOEMS* **2008**, *7*, 043002.
(37) Montgomery, D. C. *Design and Analysis of Experiments*; John Wiley & Sons, Inc., 2006.
(38) Leonard, D. N.; Chandler, G. W.; Seraphin, S. Scanning Electron Microscopy. In *Characterization of Materials*; John Wiley & Sons, Inc., 2002. DOI: 10.1002/0471266965.com081.pub2.
(39) Frank, O.; Zukalova, M.; Laskova, B.; Kürti, J.; Koltai, J.; Kavan, L. Raman Spectra of Titanium Dioxide (Anatase, Rutile) with Identified Oxygen Isotopes (16, 17, 18). *Phys. Chem. Chem. Phys.* **2012**, *14* (42), 14567−14572.
(40) Ding, X. Z.; Qi, Z. A.; He, Y. Z. Effect of Tin Dioxide Doping on Rutile Phase Formation in Sol-Gel-Derived Nanocrystalline Titania Powders. *Nanostruct. Mater.* **1994**, *4* (6), 663−668.
(41) Mueller, J. B.; Fischer, J.; Mayer, F.; Kadic, M.; Wegener, M. Polymerization Kinetics in Three-Dimensional Direct Laser Writing. *Adv. Mater.* **2014**, *26* (38), 6566−6571.
(42) Mueller, J. B.; Fischer, J.; Mange, Y. J.; Nann, T.; Wegener, M. In-Situ Local Temperature Measurement during Three-Dimensional Direct Laser Writing. *Appl. Phys. Lett.* **2013**, *103* (12), 123107.

https://dx.doi.org/10.1021/acs.nanolett.0c00454
Nano Lett. 2020, 20, 3513−3520